Control of Nonprehensile Planar Rolling Manipulation: A Passivity-Based Approach

Diana Serra, Fabio Ruggiero, *Member, IEEE,* Alejandro Donaire, *Member, IEEE,* Luca Rosario Buonocore, Vincenzo Lippiello, *Senior Member, IEEE,* and Bruno Siciliano, *Fellow, IEEE*.

***Abstract*—This paper presents a new procedure to design a control law using the classical interconnection and damping assignment technique within the passivity-based port-Hamiltonian framework. The sought goal is to reduce the complexity of solving the so-called matching equations. The proposed approach is applied to two case studies of planar rolling nonprehensile manipulation. Namely, the ball-and-beam and the eccentric disk-on-disk. The performance of the resulting controllers is illustrated through both simulations and experimental results, showing the applicability of the design in a real set-up.**

***Index Terms*—Nonprehensile rolling manipulation, passivity-based control, dynamic manipulation, underactuated systems.**

I. Introduction

Port-Hamiltonian (pH) formalism has gained the attention of the control and robotics research communities in the last decade as a methodology for modeling and control design of complex system [1], [2], [3], [4], [5]. Rooted in the classical mechanics, the pH formalism is a representation of the system dynamics that explicitly reveals energy and physical properties related to the energy exchange, power flow, and interconnection structure. Such physical information is exploited for the design of control algorithms within non-negligible dynamics tasks. In particular, the method of *interconnection and damping assignment passivity-based control* (IDA-PBC) is here considered [2], [5]. The IDA-PBC aims at finding a control law such that the closed loop preserves the Hamiltonian structure, with a minimum of the potential energy at the desired equilibrium, and a further damping injection to ensure asymptotic stability. The IDA-PBC method differs from other nonlinear control methodologies, typically applied in robotics, such as feedback linearization, where a linear dynamics is imposed at the expense of exact-cancelation of the nonlinear system dynamics, which may cause robustness problems. The control law is then obtained by matching the open-loop and desired closed-loop dynamics. Such a match is guaranteed by solving a set of partial differential equations (PDEs), the so-called *matching equations*, which is also a bottleneck of the IDA-PBC approach despite the existence of constructive and explicit solutions for many structured problems (e.g. [6], [7], [8]).

In this work, a new procedure to solve the matching equations for a class of mechanical systems is proposed. The carried out approach reduces the complexity of the IDA-PBC design, while preserving its effectiveness. Under certain conditions, the proposed method consists in giving the explicit solution of a subset of PDEs resulting from the matching equations, while transforming the remaining PDEs in a set of algebraic equations. This novel procedure for the IDA-PBC design can be applied to underactuated planar mechanical systems with separable and non-separable Hamiltonians, *i.e.*, with constant and non-constant mass matrix, respectively. Such class of systems includes *nonprehensile planar rolling manipulation* tasks, which are here proposed as robotic case studies to illustrate the design procedure outlined in this paper.

Nonprehensile planar rolling manipulation systems address those tasks that involve an actuated manipulator referred to as hand, and an object which is manipulated without form or force closure grasps [9]. The *disk-on-disk* [1], [10], [11], the *ball-and-beam* [12], [13], [14], [15], and the *butterfly robot* [16], [17], [18] are some robotic benchmarks used to simulate different nonprehensile planar rolling manipulation tasks. In detail, the disk-on-disk is composed of an upper disk (object) free to roll without slipping on the rim of a lower actuated disk (hand). The ball-and-beam consists of a beam (hand) actuated by a torque around its center of mass (CoM) together with a ball (object) rolling on it. The butterfly robot is composed of an actuated butterfly-shaped link (hand) on whose rim a ball (object) can freely roll. In all these cases the control objective is to balance the object and drive the hand towards the desired configuration. In this paper, two nonprehensile planar rolling robotic systems with non-separable Hamiltonian are considered as case studies: the ball-and-beam and the *eccentric disk-on-disk*. This last example is a variant of the disk-on-disk system, where the center of rotation of the hand and its geometric center are not coincident. Simulation tests on the ball-and-beam, and experiments on the real physical prototype of the eccentric disk-on-disk system are presented to confirm the performance of the proposed control methodology.

The outline of the paper is as follows. Next section highlights the novelties proposed within this work. Existing control designs for the selected case studies are described in Section III. A summary of the IDA-PBC is presented in Section IV. The main result of this work is shown in Section V. The general dynamic model for nonprehensile planar rolling

The research leading to these results has been supported by the RoDyMan project, which has received funding from the European Research Council FP7 Ideas under Advanced Grant agreement number 320992. The authors are solely responsible for the content of this manuscript.

D. Serra, F. Ruggiero, V. Lippiello and B. Siciliano are with CREATE Consortium and with Department of Electrical Engineering and Information Technology, University of Naples Federico II, via Claudio 21, 80125, Naples, Italy. A. Donaire is with The University of Newcastle, University Dr, 2308, Callaghan, NSW, Australia. L.R. Buonocore is with CERN, Route de Meyrin 385, Geneve 23, Switzerland.

Manuscript received May 2, 2018; revised October 18, 2018.

manipulation systems is derived in Section VI. The ball-and-beam and the eccentric disk-on-disk case studies are deeply analyzed in Section VII and Section VIII, respectively. Section IX concludes the paper.

II. Novelties

As it will be detailed in Section IV, the matching equations are split into two subsets of PDEs, namely the kinetic and the potential energy matching equations. In this paper, under certain conditions and through a suitable parametrization of the desired closed-loop mass matrix, an explicit solution is provided for the potential energy matching equation. This new procedure reduces the complexity of the IDA-PBC design by simultaneously finding the desired potential energy function for the closed-loop system and simplifying the choice of the desired mass matrix. Once the solution of the potential energy matching equation is found, the procedure to solve the kinetic energy matching equation takes inspiration from [19], without solving any PDEs.

The approach here proposed differs from [3] where the PDEs derived from the kinetic energy matching condition are transformed into a set of ordinary differential equations (ODEs). Moreover, in [3] and [14], a necessary condition for the validity of the methods is that the mass matrix of the system depends only on the unactuated variable. Differently, in the proposed control approach, the open-loop mass matrix and the desired closed-loop mass matrix can be dependent on both actuated and unactuated variables.

It is worth underlining that the proposed control approach can be applied to many two-dimensional underactuated mechanical systems having the structure outlined in Section V. Nonprehensile planar rolling manipulation systems fit into such a class. Therefore, the generalized dynamic model of nonprehensile rolling between arbitrary shapes in 2D, presented in [20], is extended by formulating the dynamics in the pH form. Besides, the assumption that the center of actuation of the hand and its geometric center are coincident is dropped. This small technical contribution, in addition to the above-outlined control approach, overcomes the limitation in [20]. In that work, nonprehensile planar rolling manipulation systems are shown to be differentially flat only if they have a constant mass matrix (*i.e.*, a separable Hamiltonian). The method proposed in this paper, instead, can be applied to systems with both a separable and a non-separable Hamiltonian. The proposed control can be thus elected as a unifying approach to solving the stabilization problem of nonprehensile planar rolling manipulation systems. As sketched in [21], finding general strategies to settle a class of problems is yet an open issue within the nonprehensile manipulation domain.

III. Exisiting Control Designs for the Selected Case Studies

In the following, a brief the state of the art about the modeling and the control of the ball-and-beam and the eccentric disk-on-disk is provided. These case studies are considered to bolster the proposed control approach. A more comprehensive analysis about nonprehensile manipulation is tackled in [21].

On the one hand, the ball-and-beam system has been extensively studied in the past years due to its peculiar feature: it fails to have a well-defined relative degree. Hence, feedback linearization cannot be applied. The authors of [13] propose an approximate input-output linearization. Whereas, an output feedback controller is introduced in [22]. The authors of [12] show a technique for obtaining stable and robust oscillations for such system consisting in two steps: the former aims at finding a control law such that the closed loop of a reduced model of the dynamics is a second-order Hamiltonian system which presents stable oscillations; in the latter step, the controller is extended to the full system using backstepping. A control method for a redundant manipulator to balance the ball-and-beam system is showed in [15]. A force/torque sensor attached to the end-effector of the manipulator is used for estimating the ball position. Since it involves significant noise, a state-feedback controller is employed along with an observer.

On the other hand, the eccentric disk-on-disk has some characteristics that make it attractive as a benchmark. In [1] an IDA-PBC controller is designed ad-hoc via a coordinate transformation for the traditional disk-on-disk (separable Hamiltonian), but it cannot be directly extended for the eccentric disk-on-disk (non-separable Hamiltonian). It is worth noticing that the dynamic behavior and the stability properties of the eccentric disk-on-disk are similar to the circular ball-and-beam investigated in [23], [24], [25]. In [24], the Jordan form of the model of the circular ball-and-beam is linearized near the unstable equilibrium to design a linear controller. A linear control approach is also used in [23], where the limits of the beam actuator are taken into account. A geometric passivity-based control approach for this system is presented in [25]. Also in that work, the authors propose a technique to avoid the solution of the matching conditions. Nevertheless, the gyroscopic term is not addressed for the control design within [25], since the energy shaping is applied to a modified dynamics resulting from a geometric feedback transformation.

IV. IDA-PBC in a Nutshell

The pH framework allows modeling of mechanical systems including the information about the energy transfer explicitly. The canonical Hamiltonian equations of motion are

$$\begin{bmatrix}\dot{\boldsymbol{q}}\\ \dot{\boldsymbol{p}}\end{bmatrix} = \begin{bmatrix}\mathbf{O}_n & \boldsymbol{I}_n\\ -\boldsymbol{I}_n & \mathbf{O}_n\end{bmatrix}\nabla\mathcal{H}(\boldsymbol{q},\boldsymbol{p}) + \begin{bmatrix}\mathbf{O}_{n\times m}\\ \boldsymbol{G}(\boldsymbol{q})\end{bmatrix}\boldsymbol{u}, \qquad (1)$$

where $\boldsymbol{q} \in \mathbb{R}^n$ is the configuration vector, $\boldsymbol{p} \in \mathbb{R}^n$ is the momenta vector, $\boldsymbol{u} \in \mathbb{R}^m$ is the control input, $\boldsymbol{G}(\boldsymbol{q}) \in \mathbb{R}^{n\times m}$ is the input mapping vector, $\boldsymbol{I}_n, \mathbf{O}_n \in \mathbb{R}^{n\times n}$ are the identity and the zero matrices, respectively, and $\mathbf{O}_{n\times m} \in \mathbb{R}^{n\times m}$ is a $n\times m$ matrix with all-zero entries. The function $\mathcal{H} : \mathbb{R}^{2n} \to \mathbb{R}$ is the Hamiltonian, which represents the total energy (kinetic plus potential) stored in the system, having the form

$$\mathcal{H}(\boldsymbol{q},\boldsymbol{p}) = \frac{1}{2}\boldsymbol{p}^T\boldsymbol{M}^{-1}(\boldsymbol{q})\boldsymbol{p} + V(\boldsymbol{q}),$$

where $V(\boldsymbol{q}) \in \mathbb{R}$ is the potential energy function and $\boldsymbol{M}(\boldsymbol{q}) = \boldsymbol{M}^T(\boldsymbol{q}) \in \mathbb{R}^{n\times n}$ is the positive-definite mass matrix.

Stabilization of (1) to the desired equilibrium $(\boldsymbol{q},\boldsymbol{p}) = (\boldsymbol{q}^\star, \mathbf{0}_n)$, where $\mathbf{0}_n \in \mathbb{R}^n$ is the zero vector, is achieved using

the IDA-PBC by assigning the target dynamics to the closed loop [14]

$$\begin{bmatrix}\dot{\boldsymbol{q}}\\ \dot{\boldsymbol{p}}\end{bmatrix} = \begin{bmatrix}\mathbf{O}_n & \boldsymbol{M}^{-1}(\boldsymbol{q})\boldsymbol{M}_d(\boldsymbol{q})\\ -\boldsymbol{M}_d(\boldsymbol{q})\boldsymbol{M}^{-1}(\boldsymbol{q}) & \boldsymbol{J}_2(\boldsymbol{q},\boldsymbol{p})\end{bmatrix}\nabla\mathcal{H}_d(\boldsymbol{q},\boldsymbol{p}), \tag{2}$$

where $\boldsymbol{J}_2(\boldsymbol{q},\boldsymbol{p}) \in \mathbb{R}^{n\times n}$ is the desired interconnection matrix, and $\boldsymbol{M}_d(\boldsymbol{q}) \in \mathbb{R}^{n\times n}$ the desired mass matrix. The desired total energy function is given by

$$\mathcal{H}_d(\boldsymbol{q},\boldsymbol{p}) = \frac{1}{2}\boldsymbol{p}^T\boldsymbol{M}_d^{-1}(\boldsymbol{q})\boldsymbol{p} + V_d(\boldsymbol{q}),$$

with $V_d(\boldsymbol{q}) \in \mathbb{R}$ the desired potential energy function. Then, $(\boldsymbol{q}^\star, \mathbf{0}_n)$ will be a stable equilibrium configuration of the closed-loop (2) if

C.1 $\boldsymbol{M}_d(\boldsymbol{q})$ is symmetric and positive definite;
C.2 $\boldsymbol{q}^\star = \arg\min V_d(\boldsymbol{q})$;
C.3 $\boldsymbol{J}_2(\boldsymbol{q},\boldsymbol{p})$ is skew-symmetric.

The stabilization of the desired equilibrium is achieved by identifying the class of Hamiltonian systems that can be obtained via feedback. The conditions under which this feedback law exists are the matching conditions, *i.e.*, matching the original dynamic system (1) and the target dynamic system (2):

$$\begin{aligned}&\begin{bmatrix}\mathbf{O}_n & \boldsymbol{I}_n\\ -\boldsymbol{I}_n & \mathbf{O}_n\end{bmatrix}\nabla\mathcal{H} + \begin{bmatrix}\mathbf{O}_{n\times m}\\ \boldsymbol{G}\end{bmatrix}\boldsymbol{u}\\ &\quad= \begin{bmatrix}\mathbf{O}_n & \boldsymbol{M}^{-1}\boldsymbol{M}_d\\ -\boldsymbol{M}_d\boldsymbol{M}^{-1} & \boldsymbol{J}_2\end{bmatrix}\nabla\mathcal{H}_d,\end{aligned} \tag{3}$$

where the dependency of the functions on their argument has been drop to simplify the notation. The first line in (3) is straightforwardly satisfied, while the second line in (3) corresponds to the following set of PDEs

$$\begin{aligned}\boldsymbol{G}^\perp\big(&\nabla_q\mathcal{H}(\boldsymbol{q},\boldsymbol{p}) - \boldsymbol{M}_d(\boldsymbol{q})\boldsymbol{M}^{-1}(\boldsymbol{q})\nabla_q\mathcal{H}_d(\boldsymbol{q},\boldsymbol{p})\\ &+ \boldsymbol{J}_2(\boldsymbol{q},\boldsymbol{p})\boldsymbol{M}_d^{-1}(\boldsymbol{q})\boldsymbol{p}\big) = 0,\end{aligned} \tag{4}$$

where $\boldsymbol{G}^\perp$ is the full rank left annihilator of $\boldsymbol{G}$. The PDEs (4) can be separated into the two subsets of PDEs:

$$\begin{aligned}\boldsymbol{G}^\perp\big(&\nabla_q(\boldsymbol{p}^T\boldsymbol{M}^{-1}(\boldsymbol{q})\boldsymbol{p})\\ &- \boldsymbol{M}_d(\boldsymbol{q})\boldsymbol{M}^{-1}(\boldsymbol{q})\nabla_q(\boldsymbol{p}^T\boldsymbol{M}_d^{-1}(\boldsymbol{q})\boldsymbol{p})\\ &+ 2\boldsymbol{J}_2(\boldsymbol{q},\boldsymbol{p})\boldsymbol{M}_d^{-1}(\boldsymbol{q})\boldsymbol{p}\big) = 0,\end{aligned} \tag{5}$$

$$\boldsymbol{G}^\perp\big(\nabla_q V(\boldsymbol{q}) - \boldsymbol{M}_d(\boldsymbol{q})\boldsymbol{M}^{-1}(\boldsymbol{q})\nabla_q V_d(\boldsymbol{q})\big) = 0, \tag{6}$$

where (5) and (6) are the kinetic and the potential energy matching equations, respectively. By solving (5)-(6) for $\boldsymbol{M}_d(\boldsymbol{q})$, $V_d(\boldsymbol{q})$ and $\boldsymbol{J}_2(\boldsymbol{q},\boldsymbol{p})$, subject to **C.1**, **C.2**, and **C.3**, the energy shaping control is given by

$$\begin{aligned}\boldsymbol{u}_{es} = (\boldsymbol{G}^T\boldsymbol{G})^{-1}\boldsymbol{G}^T(&\nabla_q\mathcal{H}(\boldsymbol{q},\boldsymbol{p})\\ &- \boldsymbol{M}_d(\boldsymbol{q})\boldsymbol{M}^{-1}(\boldsymbol{q})\nabla_q\mathcal{H}_d(\boldsymbol{q},\boldsymbol{p}) + \boldsymbol{J}_2(\boldsymbol{q},\boldsymbol{p})\boldsymbol{M}_d^{-1}(\boldsymbol{q})\boldsymbol{p}).\end{aligned} \tag{7}$$

It is worth remarking that not every desired $\boldsymbol{M}_d(\boldsymbol{q})$, $V_d(\boldsymbol{q})$ and $\boldsymbol{J}_2(\boldsymbol{q},\boldsymbol{p})$ can be chosen, but only those solving (5)-(6) subject to the conditions **C.1**, **C.2**, and **C.3**.

By applying (7) to the Hamiltonian dynamics (1), the closed-loop target dynamics (2) is obtained. Damping aimed at achieving asymptotic stability is then injected through

$$\boldsymbol{u}_{di} = -\boldsymbol{K}_v\boldsymbol{G}^T\nabla_p\mathcal{H}_d(\boldsymbol{q},\boldsymbol{p}), \tag{8}$$

where $\boldsymbol{K}_v \in \mathbb{R}^{m\times m}$ is a symmetric and positive definite matrix. The damping injection (8) and the energy shaping control (7) are then assembled to generate the IDA-PBC

$$\boldsymbol{u} = \boldsymbol{u}_{es} + \boldsymbol{u}_{di}. \tag{9}$$

Therefore, through this adjustement, the closed-loop dynamics (2) is modified as follows

$$\begin{bmatrix}\dot{\boldsymbol{q}}\\ \dot{\boldsymbol{p}}\end{bmatrix} = \begin{bmatrix}\mathbf{O}_n & \boldsymbol{M}^{-1}(\boldsymbol{q})\boldsymbol{M}_d(\boldsymbol{q})\\ -\boldsymbol{M}_d(\boldsymbol{q})\boldsymbol{M}^{-1}(\boldsymbol{q}) & \boldsymbol{J}_2(\boldsymbol{q},\boldsymbol{p}) - \boldsymbol{R}_d\end{bmatrix}\nabla\mathcal{H}_d(\boldsymbol{q},\boldsymbol{p}), \tag{10}$$

in which dependencies have been dropped, and $\boldsymbol{R}_d = \boldsymbol{G}\boldsymbol{K}_v\boldsymbol{G}^T \in \mathbb{R}^{n\times n}$ is the positive-(semi)definite dissipation matrix [4], [14].

V. Main Result

Consider the class of underactuated Hamiltonian systems (1) with $n = 2$, $m = 1$, $\boldsymbol{G} = \boldsymbol{e}_1 = \begin{bmatrix}1 & 0\end{bmatrix}^T$, and, consequently, $\boldsymbol{G}^\perp = \boldsymbol{e}_2^T = \begin{bmatrix}0 & 1\end{bmatrix}$. The first step towards the proposed resolution to solve the matching conditions is related to the potential energy PDEs and the conditions of symmetry and positive definiteness of the desired closed-loop mass matrix. Let $\boldsymbol{q} = \begin{bmatrix}q_1 & q_2\end{bmatrix}^T$ be the configuration vector, and let

$$\boldsymbol{M}(\boldsymbol{q}) = \begin{bmatrix}b_{11}(\boldsymbol{q}) & b_{12}(\boldsymbol{q})\\ b_{12}(\boldsymbol{q}) & b_{22}(\boldsymbol{q})\end{bmatrix} \tag{11}$$

be the expression of the mass matrix in (1). To look for a solution of the potential energy matching equation, the desired inertia matrix is parametrized as follows

$$\boldsymbol{M}_d(\boldsymbol{q},\boldsymbol{c}_1) = \Delta\begin{bmatrix}a_{11}(\boldsymbol{q},\boldsymbol{c}_1) & a_{12}(\boldsymbol{q},\boldsymbol{c}_1)\\ a_{12}(\boldsymbol{q},\boldsymbol{c}_1) & a_{22}(\boldsymbol{q},\boldsymbol{c}_1)\end{bmatrix}, \tag{12}$$

where $\Delta = b_{11}(\boldsymbol{q})b_{22}(\boldsymbol{q}) - b_{12}^2(\boldsymbol{q}) > 0$ is the determinant of $\boldsymbol{M}(\boldsymbol{q})$, and $\boldsymbol{c}_1 \in \mathbb{R}^{n_{c1}}$ is a set of gains, with $n_{c1} \geq 0$, useful to design the controller. Under this assumption, the potential energy matching equation (6) becomes

$$\boldsymbol{e}_2^T\left(\nabla_q V(\boldsymbol{q}) - \boldsymbol{\Gamma}(\boldsymbol{q})\nabla_q V_d(\boldsymbol{q},\boldsymbol{c}_2)\right) = 0, \tag{13}$$

where $\boldsymbol{c}_2 \in \mathbb{R}^{n_{c2}}$ is a set of gains, with $n_{c2} \geq 0$, useful to design the controller, and

$$\boldsymbol{\Gamma}(\boldsymbol{q},\boldsymbol{c}_1) = \begin{bmatrix}a_{11}b_{22} - a_{12}b_{12} & a_{12}b_{11} - a_{11}b_{12}\\ a_{12}b_{22} - a_{22}b_{12} & a_{22}b_{11} - a_{12}b_{12}\end{bmatrix}. \tag{14}$$

The PDE (13) can be equivalently written as

$$\nabla_{q_2}V(\boldsymbol{q}) + \alpha(\boldsymbol{q})\nabla_{q_1}V_d(\boldsymbol{q},\boldsymbol{c}_2) + \beta(\boldsymbol{q})\nabla_{q_2}V_d(\boldsymbol{q},\boldsymbol{c}_2) = 0. \tag{15}$$

with

$$\begin{aligned}\alpha(\boldsymbol{q},\boldsymbol{c}_1) &= a_{22}(\boldsymbol{q},\boldsymbol{c}_1)b_{12}(\boldsymbol{q}) - a_{12}(\boldsymbol{q},\boldsymbol{c}_1)b_{22}(\boldsymbol{q}),\\ \beta(\boldsymbol{q},\boldsymbol{c}_1) &= a_{12}(\boldsymbol{q},\boldsymbol{c}_1)b_{12}(\boldsymbol{q}) - a_{22}(\boldsymbol{q},\boldsymbol{c}_1)b_{11}(\boldsymbol{q}).\end{aligned} \tag{16}$$

The main advantage of the proposed approach is the use of the scalar functions $\alpha(\boldsymbol{q},\boldsymbol{c}_1)$ and $\beta(\boldsymbol{q},\boldsymbol{c}_1)$. A suitable choice

of these functions allows the possibility to have an explicit solution of (15) (see Appendix I). Notice that the form of $\alpha(\boldsymbol{q}, \boldsymbol{c}_1)$ and $\beta(\boldsymbol{q}, \boldsymbol{c}_1)$, and the gains $\boldsymbol{c}_1$ and $\boldsymbol{c}_2$, are selected such that $V_d(\boldsymbol{q}, \boldsymbol{c}_2)$ satisfies **C.2**. Once $\alpha(\boldsymbol{q}, \boldsymbol{c}_1)$, $\beta(\boldsymbol{q}, \boldsymbol{c}_1)$, $\boldsymbol{c}_1$ and $\boldsymbol{c}_2$ are chosen, the terms $a_{12}(\boldsymbol{q}, \boldsymbol{c}_1)$ and $a_{22}(\boldsymbol{q}, \boldsymbol{c}_1)$ of the desired mass matrix are retrieved as

$$a_{12}(\boldsymbol{q}.\boldsymbol{c}_1) = -\frac{\alpha(\boldsymbol{q}, \boldsymbol{c}_1) b_{11}(\boldsymbol{q}) + \beta(\boldsymbol{q}, \boldsymbol{c}_1) b_{12}(\boldsymbol{q})}{\Delta}, \qquad (17)$$
$$a_{22}(\boldsymbol{q}, \boldsymbol{c}_1) = -\frac{\alpha(\boldsymbol{q}, \boldsymbol{c}_1) b_{12}(\boldsymbol{q}) + \beta(\boldsymbol{q}, \boldsymbol{c}_1) b_{22}(\boldsymbol{q})}{\Delta}.$$

Through this choice, the proposed desired closed-loop mass matrix is structurally symmetric, while the condition **C.1** is fulfilled only if $a_{11}(\boldsymbol{q}, \boldsymbol{c}_1) > 0$ and $a_{11}(\boldsymbol{q}, \boldsymbol{c}_1) a_{22}(\boldsymbol{q}, \boldsymbol{c}_1) - a_{12}^2(\boldsymbol{q}, \boldsymbol{c}_1) > 0$. Therefore, by selecting a_{11} as

$$a_{11}(\boldsymbol{q}, \boldsymbol{c}_1) = \frac{k_a a_{12}^2(\boldsymbol{q}, \boldsymbol{c}_1)}{a_{22}(\boldsymbol{q}, \boldsymbol{c}_1)} > 0, \qquad (18)$$

where $k_a > 1$ is a constant parameter, the conditions for $\boldsymbol{M}_d$ to be positive definite are met if

$$\alpha(\boldsymbol{q}, \boldsymbol{c}_1) b_{12}(\boldsymbol{q}) + \beta(\boldsymbol{q}, \boldsymbol{c}_1) b_{22}(\boldsymbol{q}) < 0. \qquad (19)$$

Hence, the gains $\boldsymbol{c}_1$ have to be chosen to fulfil (19) without destroying the conditions found to satisfy **C.2**. If this is possible, then the desired mass matrix takes the form

$$\boldsymbol{M}_d(\boldsymbol{q}) = \begin{bmatrix} -\dfrac{k_a(\alpha b_{11} + \beta b_{12})^2}{(\alpha b_{12} + \beta b_{22})} & -(\alpha b_{11} + \beta b_{12}) \\ -(\alpha b_{11} + \beta b_{12}) & -(\alpha b_{12} + \beta b_{22}) \end{bmatrix}, \qquad (20)$$

otherwise it is necessary to re-design $\alpha(\boldsymbol{q}, \boldsymbol{c}_1)$ and $\boldsymbol{\beta}(\boldsymbol{q}, \boldsymbol{c}_1)$ and find another solution for (15).

Subsequently, the degree of freedom given by the matrix $\boldsymbol{J}_2(\boldsymbol{q}, \boldsymbol{p})$ is used to satisfy the kinetic energy matching equation (5). The approach proposed by [19] is followed to deal with the kinetic energy matching equation without solving any PDE again. The interconnection matrix $\boldsymbol{J}_2$ is chosen through the following structure

$$\boldsymbol{J}_2(\boldsymbol{q}, \boldsymbol{p}) = \begin{bmatrix} 0 & j_2(\boldsymbol{q}, \boldsymbol{p}) \\ -j_2(\boldsymbol{q}, \boldsymbol{p}) & 0 \end{bmatrix}. \qquad (21)$$

Since $\boldsymbol{e}_2^T \boldsymbol{J}_2(\boldsymbol{q}, \boldsymbol{p}) = -j_2(\boldsymbol{q}, \boldsymbol{p}) \boldsymbol{e}_1^T$, the kinetic energy matching condition (5) can be expressed as

$$\begin{aligned} &\boldsymbol{e}_2^T \nabla_q (\boldsymbol{p}^T \boldsymbol{M}^{-1}(\boldsymbol{q}) \boldsymbol{p}) \\ &- \boldsymbol{e}_2^T \boldsymbol{M}_d(\boldsymbol{q}) \boldsymbol{M}^{-1}(\boldsymbol{q}) \nabla_q (\boldsymbol{p}^T \boldsymbol{M}_d^{-1}(\boldsymbol{q}) \boldsymbol{p}) \\ &- 2 j_2(\boldsymbol{q}, \boldsymbol{p}) \boldsymbol{e}_1^T \boldsymbol{M}_d^{-1}(\boldsymbol{q}) \boldsymbol{p} = 0. \end{aligned} \qquad (22)$$

The scalar function $j_2(\boldsymbol{q}, \boldsymbol{p})$ can be obtained solving (22) as an algebraic equation

$$\begin{aligned} j_2(\boldsymbol{q}, \boldsymbol{p}) = &\left(2 \boldsymbol{e}_1^T \boldsymbol{M}_d^{-1}(\boldsymbol{q}) \boldsymbol{p}\right)^{-1} \left(\boldsymbol{e}_2^T \nabla_q (\boldsymbol{p}^T \boldsymbol{M}^{-1}(\boldsymbol{q}) \boldsymbol{p}) \right. \\ &\left. - \boldsymbol{e}_2^T \boldsymbol{M}_d(\boldsymbol{q}) \boldsymbol{M}^{-1}(\boldsymbol{q}) \nabla_q (\boldsymbol{p}^T \boldsymbol{M}_d^{-1}(\boldsymbol{q}) \boldsymbol{p})\right). \end{aligned} \qquad (23)$$

The IDA-PBC law can be finally computed from (9). The proposed constructive solution is resumed in the flow chart depicted in Fig. 1.

The method used to satisfy the kinetic energy matching equation, inspired by [19], provides a solution that is not always well-defined. Close to the equilibrium, the numerator

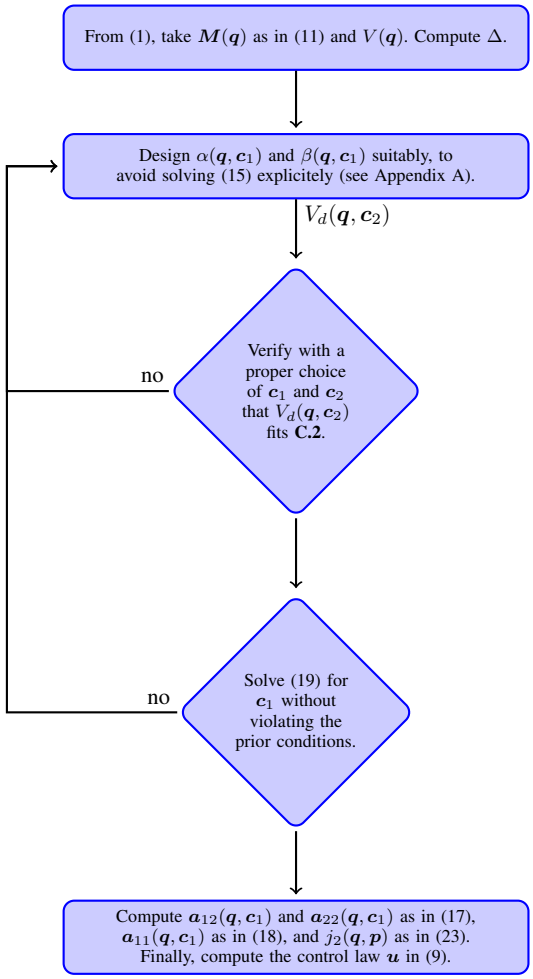

Fig. 1. Flow chart of the proposed constructive solution.

of (23), which has a quadratic dependence on $\boldsymbol{p}$, tends towards zero faster than the denominator, which depends linearly on $\boldsymbol{p}$, thus avoiding any singularity issues. Despite this, a study about the denominator of the relation (23) reveals that, far from the equilibrium, it might be nullified if the equality $(\alpha(\boldsymbol{q}, \boldsymbol{c}_1) b_{12}(\boldsymbol{q}) + \beta(\boldsymbol{q}, \boldsymbol{c}_1) b_{22}(\boldsymbol{q})) p_1 = (\alpha(\boldsymbol{q}, \boldsymbol{c}_1) b_{11}(\boldsymbol{q}) + \beta(\boldsymbol{q}, \boldsymbol{c}_1) b_{12}(\boldsymbol{q})) p_2$ holds, with $\boldsymbol{p} = \begin{bmatrix} p_1 & p_2 \end{bmatrix}^T$. This situation is addressed in practice by saturating the denominator of (23) when its absolute value is under a small enough threshold. The simplification of the design proposed here is at the expense of the presence of possible singular solutions of (23), but these can always be numerically managed in the controller implementation.

Remark. The main result of this section can be thus applied to any underactuated mechanical system, with both separable and non-separable Hamiltonians, whose dynamic model can be expressed as in (1) with $n = 2$, $m = 1$, $\boldsymbol{G} = \boldsymbol{e}_1$.

VI. Dynamic Model of Nonprehensile Planar Rolling Manipulation Systems

In this section, the dynamic model of nonprehensile planar rolling systems is derived in the pH form. This formulation extends the works in [1], [11], [20] by removing the somewhat

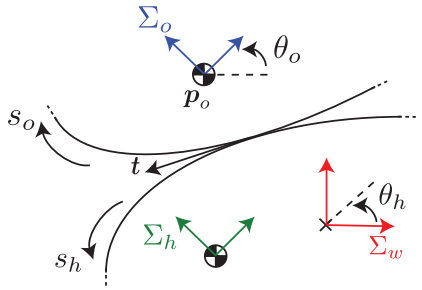

Fig. 2. A general nonprehensile planar rolling manipulation system with the center of rotation of the hand (indicated by the $\times$ symbol) not corresponding to its center of mass. The world fixed frame Σ_w is in red. The hand frame Σ_h and the object frame Σ_o, in green and blue, respectively, are placed at their respective centres of mass.

restrictive assumption that the hand can only rotate around its center of mass, which allows considering a more general class of tasks as shown in Fig. 2. Consider the inertial world fixed frame Σ_w, which is without loss of generality attached to the holder where the hand is actuated (*i.e.*, the center of rotation of the hand). Also, let Σ_h be the frame attached to the center of mass (CoM) of the hand, while Σ_o is the frame attached to the CoM of the object. Let $\theta_h \in \mathbb{R}$ be the angle of the hand in Σ_w, while $\boldsymbol{p}_o \in \mathbb{R}^2$ and $\theta_o \in \mathbb{R}$ are the position and the orientation, respectively, of Σ_o in Σ_w (see Fig. 2). The shapes of both the object and the hand are represented by an arclength parametrization: $s_h \in \mathbb{R}$ and $s_o \in \mathbb{R}$ are the arclength parameters for the hand and the object, respectively. At least locally, the shapes should be of class $\mathcal{C}^2$. Any point of the hand shape is given by the chart $\boldsymbol{c}_h^h(s_h) = \begin{bmatrix} u_h(s_h) & v_h(s_h) \end{bmatrix}^T \in \mathbb{R}^2$, expressed with respect to Σ_h, while any point of the object shape is given by $\boldsymbol{c}_o^o(s_o) = \begin{bmatrix} u_o(s_o) & v_o(s_o) \end{bmatrix}^T \in \mathbb{R}^2$, expressed with respect to Σ_o. Notice that s_h increases counterclockwise along the hand, while s_o increases clockwise along the object. With this choice, the pure rolling assumption is $\dot{s}_h = \dot{s}_o$. Without loss of generality, the frames Σ_w and Σ_h coincide at $\theta_h = 0$, the point $s_h = 0$ is at the intersection between the vertical (gravitational) axis of Σ_w and the hand shape (*i.e.*, $\boldsymbol{c}_h(0) = \begin{bmatrix} 0 & v_h(0) \end{bmatrix}^T$ in Σ_w), and thus $s_h = s_o$ at all times during rolling. Therefore, the contact location will be specified only by s_h throughout the remainder of the paper. As the first assumption, the hand and the object maintain pure rolling contact for all time. The arclength parametrization implies the property $\|\boldsymbol{c}_h^{h\prime}\| = 1$, with the symbol $'$ indicating the derivative with respect to the parameter s_h. The same holds for $\boldsymbol{c}_o^o(s_h)$. At the contact point $\boldsymbol{c}_h^h(s_h)$, the tangent vector to the shapes is expressed as $\boldsymbol{t}^h(s_h) = \boldsymbol{c}_h^{h\prime} \in \mathbb{R}^2$ forming an angle $\phi_h(s_h) = \operatorname{atan2}(v_h'(s_h), u_h'(s_h))$ in Σ_h. The same tangent can be expressed with respect to Σ_o with an angle $\phi_o(s_h) = \operatorname{atan2}(v_o'(s_h), u_o'(s_h))$. The signed curvatures of the shapes are defined as: $\kappa_h(s_h) = \phi_h'(s_h) = u_h'(s_h)v_h''(s_h) - u_h''(s_h)v_h'(s_h)$, $\kappa_o(s_h) = \phi_o'(s_h) = u_o'(s_h)v_o''(s_h) - u_o''(s_h)v_o'(s_h)$. The relative curvature at the contact point is given by

$$\kappa_r(s_h) = \kappa_h(s_h) - \kappa_o(s_h). \tag{24}$$

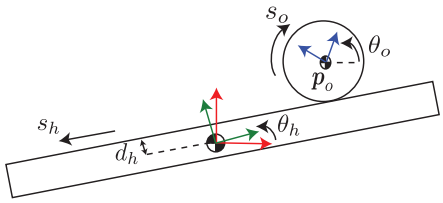

Fig. 3. A representation of the ball-and-beam system. The world fixed frame Σ_w is in red. The hand frame Σ_h and the object frame Σ_o, in green and blue, respectively, are placed at their respective centres of mass.

Notice that $\kappa_h(s_h) > 0$ and $\kappa_o(s_h) < 0$ denote convexity at the contact point for the hand and the object, respectively. Hence, $\kappa_r(s_h) > 0$ guarantees a single contact point at least locally [11]. The following constraint expresses the angle of the tangent $\boldsymbol{t}^h(s_h)$ with respect to Σ_w: $\theta_h + \phi_h(s_h) = \theta_o + \phi_o(s_h)$. Therefore, taking into account (24), the following relations hold

$$\theta_o = \theta_h + \phi_h(s_h) - \phi_o(s_h), \tag{25a}$$
$$\dot{\theta}_o = \dot{\theta}_h + \kappa_r(s_h)\dot{s}_h. \tag{25b}$$

Assuming that $\boldsymbol{R}(\theta) \in SO(2)$ is the rotation matrix in the 2D space, notice that the relation $\dot{\boldsymbol{R}}(\theta) = \boldsymbol{R}(\bar{\theta})\dot{\theta}$ holds with $\bar{\theta} = \theta + \frac{\pi}{2}$. The position of the CoM of the hand in Σ_w is denoted by $\boldsymbol{p}_h(\theta_h) = \begin{bmatrix} u_w(\theta_h) & v_w(\theta_h) \end{bmatrix}^T \in \mathbb{R}^2$. The coincidence between the contact points on both the hand and the object is expressed by $\boldsymbol{p}_h(\theta_h) + \boldsymbol{R}(\theta_h)\boldsymbol{c}_h^h(s_h) = \boldsymbol{p}_o + \boldsymbol{R}(\theta_o)\boldsymbol{c}_o^o(s_h)$, yielding to the equation $\boldsymbol{p}_o = \boldsymbol{p}_h(\theta_h) + \boldsymbol{R}(\theta_h)\boldsymbol{c}_h^h(s_h) - \boldsymbol{R}(\theta_o)\boldsymbol{c}_o^o(s_h)$, and, consequently, $\dot{\boldsymbol{p}}_o = \boldsymbol{\gamma}(\boldsymbol{q})\dot{\theta}_h + \boldsymbol{\eta}(\boldsymbol{q})\dot{s}_h = \begin{bmatrix} \boldsymbol{\gamma}(\boldsymbol{q}) & \boldsymbol{\eta}(\boldsymbol{q}) \end{bmatrix} \dot{\boldsymbol{q}}$, with

$$\boldsymbol{\gamma} = \boldsymbol{p}_h^{\backslash} + \boldsymbol{R}(\bar{\theta}_h)\boldsymbol{c}_h^h - \boldsymbol{R}(\bar{\theta}_o)\boldsymbol{c}_o^o, \tag{26a}$$
$$\boldsymbol{\eta} = \boldsymbol{R}(\theta_h)\boldsymbol{c}_h^{h\prime} - \boldsymbol{R}(\theta_o)\boldsymbol{c}_o^{o\prime} - \kappa_r\boldsymbol{R}(\bar{\theta}_o)\boldsymbol{c}_o^o, \tag{26b}$$

in which dependencies have been dropped, while (25b) is included and (25a) has to be plugged in. The symbol $^{\backslash}$ indicates the derivative with respect to θ_h, and the configuration vector is defined as $\boldsymbol{q} = \begin{bmatrix} \theta_h & s_h \end{bmatrix}^T$. For this class of systems the kinetic energy is given by $T = \frac{1}{2}\left(I_h\dot{\theta}_h^2 + m_h\dot{\boldsymbol{p}}_h^{\mathrm{T}}(\theta_h)\dot{\boldsymbol{p}}_h(\theta_h) + m_o\dot{\boldsymbol{p}}_o^{\mathrm{T}}\dot{\boldsymbol{p}}_o + I_o\dot{\theta}_o^2\right) = \frac{1}{2}\boldsymbol{p}^T\boldsymbol{M}^{-1}(\boldsymbol{q})\boldsymbol{p}$, with $\boldsymbol{p} = \boldsymbol{M}(\boldsymbol{q})\dot{\boldsymbol{q}}$ and the elements of the mass matrix are given by: $b_{11}(\boldsymbol{q}) = I_h + I_o + m_h\boldsymbol{p}_h^{\backslash T}\boldsymbol{p}_h^{\backslash} + m_o\boldsymbol{\gamma}^T(\boldsymbol{q})\boldsymbol{\gamma}(\boldsymbol{q})$, $b_{12}(\boldsymbol{q}) = I_o\kappa_r(s_h) + m_o\boldsymbol{\gamma}(\boldsymbol{q})^T\boldsymbol{\eta}(\boldsymbol{q})$, and $b_{22}(\boldsymbol{q}) = I_o\kappa_r^2(s_h) + m_o\boldsymbol{\eta}(\boldsymbol{q})^T\boldsymbol{\eta}(\boldsymbol{q})$. The potential energy is, instead, given by

$$V(\boldsymbol{q}) = g\boldsymbol{e}_2^T(m_o\boldsymbol{p}_o(\boldsymbol{q}) + m_h\boldsymbol{p}_h(\boldsymbol{q})). \tag{27}$$

This class of systems can be then expressed in the pH form (1), with $n = 2$, $m = 1$, $\boldsymbol{G} = \boldsymbol{e}_1$.

VII. Case Study 1: The Ball-and-Beam

The ball-and-beam is a standard benchmark belonging to the class of nonprehensile planar rolling manipulation systems. It is composed of a ball rolling on one degree of freedom linear beam. In the following, the ball-and-beam dynamic model is retrieved from the general formulation presented in Section VI. Afterwards, the procedure proposed for the IDA-PBC design

is applied. Simulations are finally performed to evaluate the performance of the controller.

A. Dynamic Model of the Ball-and-Beam

The ball-and-beam system is shown in Fig. 3. It is composed of a beam that can rotate around its CoM and a ball that can only roll along the beam. The shape of the hand (*i.e.*, the beam) is parametrized through the chart $\boldsymbol{c}_h^h(s_h) = \begin{bmatrix} -s_h & d_h \end{bmatrix}^T$, with $d_h \in \mathbb{R}^+$ a fixed distance between CoM of the beam and the surface where the ball rolls. The shape of the object (*i.e.*, the ball) is parametrized by the chart $\boldsymbol{c}_o^o(s_h) = -\rho_o \begin{bmatrix} \sin\frac{s_h}{\rho_o} & \cos\frac{s_h}{\rho_o} \end{bmatrix}^T$, with $\rho_o \in \mathbb{R}^+$ the radius of the ball. For this system, the center of rotation of the hand corresponds to its geometric center. By considering (24), the signed curvatures of the beam and the ball are $\kappa_h = 0$ and $\kappa_o = -1/\rho_o$, respectively. The relative curvature is thus given by $\kappa_r = 1/\rho_o$. The ball's angular velocity is instead given by (25b) as $\dot{\theta}_o = \dot{\theta}_h + \dfrac{\dot{s}_h}{\rho_o}$. To compute the mass matrix of the system, the vectors $\boldsymbol{\gamma}(\boldsymbol{q})$ and $\boldsymbol{\eta}(\boldsymbol{q})$ in (26) are $\boldsymbol{\gamma}(\boldsymbol{q}) = \begin{bmatrix} -(\rho_o + d_h)c_{\theta_h} + s_h s_{\theta_h} & -(\rho_o + d_h)s_{\theta_h} - s_h c_{\theta_h} \end{bmatrix}^T$, and $\boldsymbol{\eta}(\boldsymbol{q}) = -\begin{bmatrix} c_{\theta_h} & s_{\theta_h} \end{bmatrix}^T$. The resulting elements of the mass matrix are: $b_{11} = c_{b1} + c_{b2}s_h^2$, $b_{12} = \frac{I_o}{\rho_o} + m_o d_h + m_o\rho_o$, $b_{22} = \frac{I_o}{\rho_o^2} + m_o$, where $c_{b1} = I_h + I_o + m_o d_h^2 + 2m_o d_h\rho_o + m_o\rho_o^2$ and $c_{b2} = m_o$. The potential energy (27) for this system becomes $V(\boldsymbol{q}) = m_o g[(d_h + \rho_o)\cos(\theta_h) - s_h \sin(\theta_h)]$.

In the literature, it is usual to neglect the square of s_h in $b_{11}(s_h)$. This assumption holds for slow angular rates of the beam, balls with a small mass, and short beams [26], [20], but it is not included in this paper [1].

B. Control Design for the Ball-and-Beam

The sought goal is to stabilize the equilibrium $\boldsymbol{q}^\star = (0, s_h^\star)$, where $s_h^\star$ is the desired location of the ball on the beam. Following the procedure outlined in Section V, the quantities $\boldsymbol{M}(\boldsymbol{q})$ and $V(\boldsymbol{q})$ are retrieved from the previous subsection. The amount Δ can be thus computed. For this case study, the functions $\alpha(\boldsymbol{q}, \boldsymbol{c}_1)$ and $\beta(\boldsymbol{q}, \boldsymbol{c}_1)$ are designed as $\alpha(\theta_h, k) = k\sin(\theta_h)/\theta_h = k\text{sinc}(\theta_h)$ and $\beta(\theta_h) = -\text{sinc}(\theta_h)$, where $k \in \mathbb{R}$ is a gain. Notice that the sinc$(\cdot)$ function is analytic everywhere. Assuming the domain of interest as $-\pi < \theta_h < \pi$, then $0 < \text{sinc}(\theta_h) < 1$. Replacing the chosen functions in (15), the potential energy matching equation becomes

$$-m_o g \sin(\theta_h) + k\text{sinc}(\theta_h)\nabla_{\theta_h} V_d(\boldsymbol{q}) - \text{sinc}(\theta_h)\nabla_{s_h} V_d(\boldsymbol{q}) = 0. \tag{28}$$

Taking into account the results provided in the Appendix A, a solution of (28) is given by

$$V_d(\boldsymbol{q}, \boldsymbol{c}_2) = \frac{m_o g \theta_h^2}{2k} + f\left(\frac{\theta_h + k s_h}{k}, \boldsymbol{c}_2\right), \tag{29}$$

where $f(\cdot)$ is a generic function of its arguments. To satisfy **C.2**, the function $f(\cdot)$ is chosen such that the desired potential function (29) results as follows

$$V_d(\boldsymbol{q}, k_f) = \frac{m_o g \theta_h^2}{2k} - \cos\left(\frac{k_f}{k}[\theta_h + k(s_h - s_h^\star)]\right), \tag{30}$$

with $k_f \in \mathbb{R}$ a gain. To verify that $\boldsymbol{q}^\star$ is a minimum for (30), the corresponding Jacobian is firstly computed as

$$\nabla V_d(\boldsymbol{q}) = \begin{bmatrix} \frac{m_o g}{k}\theta_h + \frac{k_f}{k}\sin\left(\frac{k_f}{k}[\theta_h + k(s_h - s_h^\star)]\right) \\ k_f \sin\left(\frac{k_f}{k}[\theta_h + k(s_h - s_h^\star)]\right) \end{bmatrix}, \tag{31}$$

where it is possible to verify that $\nabla V_d(\boldsymbol{q})$ is zero at $\boldsymbol{q}^\star$. Then, the corresponding Hessian is given by

$$\nabla^2 V_d(\boldsymbol{q}) = \begin{bmatrix} \frac{m_o g}{k} + \frac{k_f^2}{k^2}\cos\phi & \frac{k_f^2}{k}\cos\phi \\ \frac{k_f^2}{k}\cos\phi & k_f^2\cos\phi \end{bmatrix}, \tag{32}$$

with $\phi = \frac{k_f}{k}(\theta_h + k(s_h - s_h^\star))$. It is possible to verify that $\nabla^2 V_d(\boldsymbol{q})$ is positive definite at the desired equilibrium $\boldsymbol{q}^\star$ if $k > 0$ and $k_f \neq 0$. Through these conditions, the desired potential function $V_d(\boldsymbol{q})$ has a minimum at the desired equilibrium $\boldsymbol{q}^\star$.

Afterwards, inequality (19) must be solved. With the choices selected above, such an inequality becomes

$$k b_{12} - b_{22} < 0, \tag{33}$$

which has the straightforward solution $k < \frac{b_{22}}{b_{12}}$. Since it is easy to verify that $\frac{b_{22}}{b_{12}} > 0$, such a solution is not in contrast with the condition $k > 0$ necessary to make $\nabla^2 V_d(\boldsymbol{q})$ positive definite. Therefore the gain k has to be chosen as $0 < k < \frac{b_{22}}{b_{12}}$.

Finally, the entries $a_{12}(\boldsymbol{q})$ and $a_{22}(\boldsymbol{q})$ of $\boldsymbol{M}_d(\boldsymbol{q})$ are computed as in (17)

$$\begin{aligned} a_{12}(\boldsymbol{q}) &= -\frac{\text{sinc}(\theta_h)(k b_{11}(s_h) - b_{12})}{\Delta}, \\ a_{22}(\boldsymbol{q}) &= -\frac{\text{sinc}(\theta_h)(k b_{12} - b_{22})}{\Delta}, \end{aligned} \tag{34}$$

while $a_{11}(\boldsymbol{q})$ is taken as in (18). Therefore, the desired mass matrix is positive definite and it can be written as follows

$$\boldsymbol{M}_d(\boldsymbol{q}) = \begin{bmatrix} -\frac{k_a \bar{b}^2}{(k b_{12} - b_{22})} & -\text{sinc}(\theta_h)\bar{b} \\ -\text{sinc}(\theta_h)\bar{b} & -\text{sinc}(\theta_h)(k b_{12} - b_{22}) \end{bmatrix}, \tag{35}$$

with $\bar{b} = k b_{11}(s_h) - b_{12}$. The kinetic energy matching equation (5) is satisfied using (23), while the IDA-PBC control law is computed from (9).

C. Simulations of the Controlled Ball-and-Beam

Numerical tests are proposed to assess the performance of the controller for the ball-and-beam case study. The values of the parameters of the dynamic model are m_o = 0.05 kg, ρ_o = 0.1 m, $I_o = m_o\rho_o^2$, d_h = 0.01 m, I_h = 0.02 m^{2}kg, and g = 9.81 m/s^2. The controller gains are instead chosen as $k = 4$, $k_a = 10$, $k_v = 10$, and $k_f = 1$. The sought goal is to stabilize the ball at the position $s_h^\star = 0$ m on the beam, that is $\boldsymbol{q}^\star = (0, 0)$. Simulations are performed in the Matlab/Simulink environment.

[1] It is worth noticing that the model here derived is slightly different from other models addressed in the literature. For example, the model in [3], [14] does not take into account the distance between CoM of the beam and the surface where the ball rolls, as instead addressed by d_h in this case study.

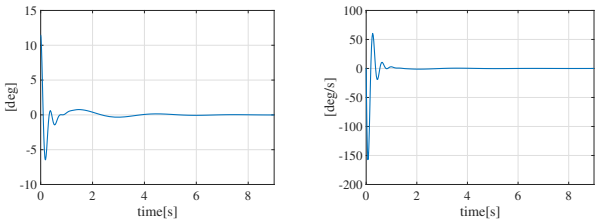

(a) Time history of $\theta_h(t)$. (b) Time history of $\dot{\theta}_h(t)$.

(c) Time history of $s_h(t)$. (d) Time history of $\dot{s}_h(t)$.

Fig. 4. Simulation test for the ball-and-beam system controlled by the proposed IDA-PBC controller.

1) Test 1: In this first test, the chosen initial conditions are $\theta_h(0) = 0.2$ rad, $\dot{\theta}_h(0) = 0.01$ rad/s, $s_h(0) = 0$ m, and $\dot{s}_h(0) = 0$ m/s.

Figure 4 shows the results obtained in this first simulation. In particular, the figure depicts the time histories of $\theta_h(t)$, $\dot{\theta}_h(t)$, $s_h(t)$, and $\dot{s}_h(t)$. The plots show that the controller can drive the states to the desired configuration while demanding a sufficiently smooth control torque.

2) Test 2: In this further test, several simulations are carried out starting the ball-and-beam system from different initial configurations. The performance of the proposed controller is evaluated through the phase portrait shown in Fig. 5. In particular, the different initial conditions $(\theta_h(0), \dot{\theta}_h(0), s_h(0), \dot{s}_h(0))$ are assigned as follows: $(0.1, 0, 0.1, 0)$ in black, $(-0.1, 0, 0.1, 0)$ in blue, $(0.1, 0, -0.1, 0)$ in red, and $(-0.1, 0, -0.1, 0)$ in green. All the trajectories arrive the origin of the phase plane, meaning that the sought goal is reached.

Besides, as an example, Fig. 6 depicts the surface of the desired potential function V_d. This exhibits a minimum at the desired equilibrium point $\boldsymbol{q}^\star$, as expected. Moreover, the red line of Fig. 6 represents the trajectory of $\theta_h(t)$ and $s_h(t)$ upon the surface of V_d when the controlled system starts at the initial condition given by $(-0.1, 0, -0.1, 0)$. The trajectory approaches the minimum of the potential energy as desired.

VIII. Case Study 2: The Eccentric Disk-on-Disk

The eccentric disk-on-disk system is composed of a disk freely rolling in full gravity upon a one degree of freedom actuated disk. The difference from the standard disk-on-disk system is given by the fact that the center of actuation does not coincide with the center of mass. Besides, the design of a stabilizing controller for the eccentric disk-on-disk is complicated by the presence of two unstable equilibrium configurations and gyroscopic forces. In the following, the

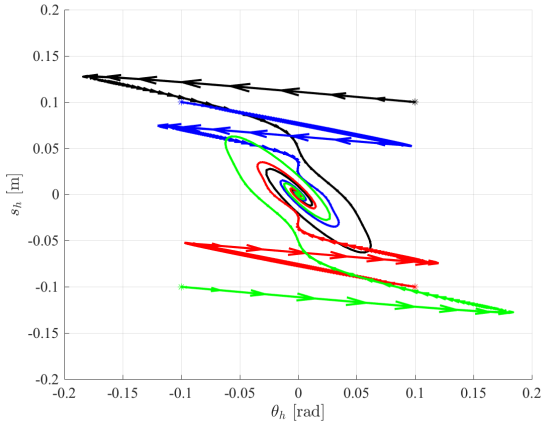

Fig. 5. Evolution of the controlled ball-and-beam system in the phase plane for different initial conditions $(\theta_h(0), \dot{\theta}_h(0), s_h(0), \dot{s}_h(0))$: $(0.1, 0, 0.1, 0)$ black line, $(-0.1, 0, 0.1, 0)$ blue line, $(0.1, 0, -0.1, 0)$ red line, $(-0.1, 0, -0.1, 0)$ green line.

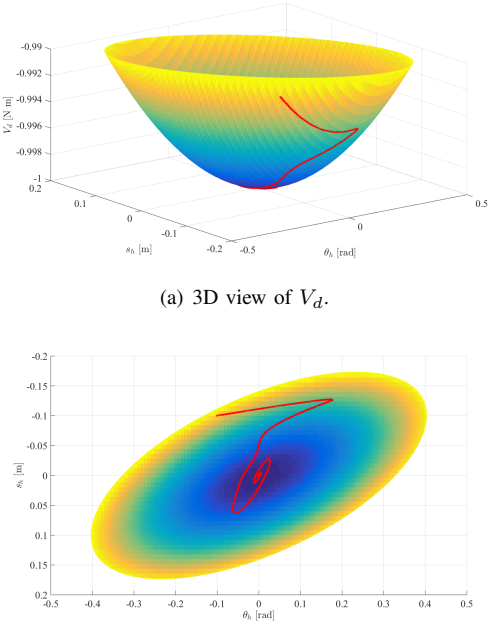

(a) 3D view of V_d.

(b) 2D view of V_d in the plane (θ_h, s_h).

Fig. 6. Surface of the desired potential function V_d with a minimum at the desired equilibrium configuration. The red line represents the 3D trajectory in the plane $\theta_h(t) - s_h(t)$ starting from initial conditions $(\theta_h(0), \dot{\theta}_h(0), s_h(0), \dot{s}_h(0)) = (-0.1, 0, -0.1, 0)$.

eccentric disk-on-disk dynamic model is retrieved from Section VI. Afterwards, the procedure proposed for IDA-PBC design is applied. Experiments are finally carried out.

A. Dynamic Model of the Eccentric Disk-on-Disk

The eccentric disk-on-disk system is represented in Fig. 7. In this system, the shape of the hand (*i.e.*, the bottom actuated disk) is parametrized through the chart $\boldsymbol{c}_h^h(s_h) = \rho_h \begin{bmatrix} -\sin\frac{s_h}{\rho_h} & \cos\frac{s_h}{\rho_h} \end{bmatrix}^T$, with $\rho_h \in \mathbb{R}^+$ the radius of the hand. The shape of the object (*i.e.*, the top disk) is parametrized by the chart $\boldsymbol{c}_o^o(s_h) = -\rho_o \begin{bmatrix} \sin\frac{s_h}{\rho_o} & \cos\frac{s_h}{\rho_o} \end{bmatrix}^T$, with $\rho_o \in \mathbb{R}^+$

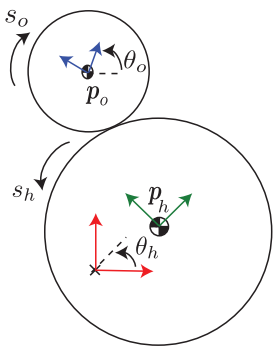

Fig. 7. A representation of the eccentric disk-on-disk system is shown in this figure. The center of rotation of the hand (indicated by the $\times$ symbol) does not correspond to its center of mass. The world fixed frame Σ_w is shown in red. The hand frame Σ_h is represented in green, while the object frame Σ_o is represented in blue. Σ_h and Σ_o are placed at the respective centers of mass.

the radius of the top disk. The position of the CoM of the hand in Σ_w is given by $\boldsymbol{p}_h(\theta_h) = \lambda \begin{bmatrix} -s_{\theta_h} & c_{\theta_h} \end{bmatrix}^T$, with $\lambda \in \mathbb{R}^-$ the distance between the center of actuation and the CoM of the hand multiplied by a minus sign, and $|\lambda| < \rho_h$. By considering (24), the relative curvature is given by $\kappa_r = \frac{\rho_h+\rho_o}{\rho_h\rho_o}$. The upper disk angular velocity is given by $\dot{\theta}_o = \dot{\theta}_h + \kappa_r \dot{s}_h$. To compute the mass matrix of the system, the vectors $\boldsymbol{\gamma}(\boldsymbol{q})$ and $\boldsymbol{\eta}(\boldsymbol{q})$ are $\boldsymbol{\gamma}(\boldsymbol{q}) = -(\rho_h + \rho_o) \begin{bmatrix} \cos\left(\theta_h + \frac{s_h}{\rho_h}\right) & \sin\left(\theta_h + \frac{s_h}{\rho_h}\right) \end{bmatrix}^T - \lambda \begin{bmatrix} c_{\theta_h} & s_{\theta_h} \end{bmatrix}^T$, and $\boldsymbol{\eta}(\boldsymbol{q}) = -\rho_o\kappa_r \begin{bmatrix} \cos\left(\theta_h + \frac{s_h}{\rho_h}\right) & \sin\left(\theta_h + \frac{s_h}{\rho_h}\right) \end{bmatrix}^T$. Therefore, the mass matrix has the following elements: $b_{11} = c_{b1} + c_{b2}\cos(\frac{s_h}{\rho_h})$, $b_{12} = c_{b3} + c_{b4}\cos(\frac{s_h}{\rho_h})$, $b_{22} = I_o\kappa_r^2 + m_o\rho_o^2\kappa_r^2$, where $c_{b1} = I_h + I_o + \lambda^2(m_h + m_o) + m_o(\rho_h + \rho_o)^2$, $c_{b2} = 2\lambda m_o(\rho_h + \rho_o)$, $c_{b3} = I_o\kappa_r + m_o\frac{(\rho_h+\rho_o)^2}{\rho_h}$, and $c_{b4} = m_o\lambda\rho_o\kappa_r$. The potential energy (27) for the eccentric disk-on-disk is given by $V(\boldsymbol{q}) = g(m_o(\rho_h + \rho_o)\cos\left(\theta_h + \frac{s_h}{\rho_h}\right) + (m_o + m_h)\lambda\cos(\theta_h))$.

B. Control Design for the Eccentric Disk-on-Disk

The sought goal is to balance the upper disk at the upright position of the hand. In this configuration, the bottom disk can present its CoM both above and below its center of actuation. With a proper change of coordinates, it is possible to express the desired equilibrium point as $\boldsymbol{q}^\star = (0, 0)$ in both cases.

Following Section V, the quantities $\boldsymbol{M}(\boldsymbol{q})$ and $V(\boldsymbol{q})$ are retrieved from the previous subsection. The amount Δ can be thus computed. The functions $\alpha(\boldsymbol{q}, \boldsymbol{c}_1)$ and $\beta(\boldsymbol{q}, \boldsymbol{c}_1)$ are designed as $\alpha(\theta_h, s_h) = \text{sinc}\left(\theta_h + \frac{s_h}{\rho_h}\right)$ and $\beta(\theta_h, s_h, k) = k\text{sinc}\left(\theta_h + \frac{s_h}{\rho_h}\right)$, where $k \in \mathbb{R}$ is a gain. Assuming the domain of interest as $-\pi < \left(\theta_h + \frac{s_h}{\rho_h}\right) < \pi$, then $0 < \text{sinc}\left(\theta_h + \frac{s_h}{\rho_h}\right) < 1$. Replacing the chosen functions in (15) yields

$$\begin{aligned} -c_v \sin\left(\theta_h + \frac{s_h}{\rho_h}\right) + \text{sinc}\left(\theta_h + \frac{s_h}{\rho_h}\right) \nabla_{\theta_h} V_d(\boldsymbol{q}) \\ + k\text{sinc}\left(\theta_h + \frac{s_h}{\rho_h}\right) \nabla_{s_h} V_d(\boldsymbol{q}) = 0, \end{aligned} \tag{36}$$

where $c_v = m_o g \frac{\rho_h+\rho_o}{\rho_h}$ is a positive parameter. Taking into account the results provided in the Appendix A, a solution of (36) is given by

$$V_d(\boldsymbol{q}, \boldsymbol{c}_2) = \frac{c_v\theta_h^2(\rho_h - k) + 2c_v\theta_h s_h}{2\rho_h} + f(s_h - k\theta_h, \boldsymbol{c}_2), \tag{37}$$

where $f(\cdot)$ is a generic function of its arguments. To satisfy **C**.2, $f(\cdot)$ is chosen such as the equation (37) becomes

$$V_d(\boldsymbol{q}, k_f) = \frac{c_v\theta_h^2(\rho_h - k) + 2c_v\theta_h s_h}{2\rho_h} + k_f(s_h - k\theta_h)^2, \tag{38}$$

where $k_f \in \mathbb{R}$ is a gain. To verify that $\boldsymbol{q}^\star$ is a minimum for (38), the corresponding Jacobian is firstly computed as

$$\nabla V_d(\boldsymbol{q}) = \begin{bmatrix} \frac{c_v(-k\theta_h + \theta_h\rho_h + s_h)}{\rho_h} + 2kk_f(k\theta_h - s_h) \\ \frac{c_v\theta_h}{\rho_h} - 2kk_f\theta_h + 2k_f s_h \end{bmatrix}, \tag{39}$$

where it is possible to verify that $\nabla V_d(\boldsymbol{q})$ is zero at $\boldsymbol{q}^\star$. Then, the corresponding Hessian is given by

$$\nabla^2 V_d(\boldsymbol{q}) = \begin{bmatrix} c_v + 2k^2k_f - \frac{c_v k}{\rho_h} & -2kk_f + \frac{c_v}{\rho_h} \\ -2kk_f + \frac{c_v}{\rho_h} & 2k_f \end{bmatrix}. \tag{40}$$

It is possible to verify that $\nabla^2 V_d(\boldsymbol{q})$ is positive definite at the desired equilibrium $\boldsymbol{q}^\star$ if $k > -\rho_h$ and $k_f > \frac{c_v}{2\rho_h(k+\rho_h)}$ Through these conditions, $V_d(\boldsymbol{q})$ has a minimum at the desired equilibrium $\boldsymbol{q}^\star$.

Afterwards, inequality (19) must be solved. With the choices selected above, such an inequality becomes

$$b_{12}(s_h) + kb_{22} < 0, \tag{41}$$

which has the straightforward solution $k < -\frac{b_{12}(s_h)}{b_{22}}$. Since it is possible to verify that $\rho_h > \frac{(c_{b3}-c_{b4})}{b_{22}}$, such a solution is not in contrast with the condition $k > -\rho_h$ necessary to make $\nabla^2 V_d(\boldsymbol{q})$ positive definite. Therefore, the gain k must be chosen as $-\rho_h < k < -\frac{c_{b3}-c_{b4}}{b_{22}}$.

Finally, the entries $a_{12}(\boldsymbol{q})$ and $a_{22}(\boldsymbol{q})$ of $\boldsymbol{M}_d(\boldsymbol{q})$ are computed as in (17)

$$\begin{aligned} a_{12}(\boldsymbol{q}) &= -\frac{\text{sinc}\left(\theta_h + \frac{s_h}{\rho_h}\right)(b_{11}(s_h) + kb_{12}(s_h))}{\Delta}, \\ a_{22}(\boldsymbol{q}) &= -\frac{\text{sinc}\left(\theta_h + \frac{s_h}{\rho_h}\right)(b_{12}(s_h) + kb_{22})}{\Delta}, \end{aligned} \tag{42}$$

while $a_{11}(\boldsymbol{q})$ is taken as in (18). The desired mass matrix is thus positive definite and it can be written as follows

$$\boldsymbol{M}_d(\boldsymbol{q}) = \begin{bmatrix} \Delta a_{11} & -h_s(b_{11} + kb_{12}) \\ -h_s(b_{11} + kb_{12}) & -h_s(b_{12} + kb_{22}) \end{bmatrix}, \tag{43}$$

where $h_s(\boldsymbol{q}) = \text{sinc}\left(\theta_h + \frac{s_h}{\rho_h}\right)$. The kinetic energy matching equation (5) is satisfied using (23), while the IDA-PBC control law is computed from (9).

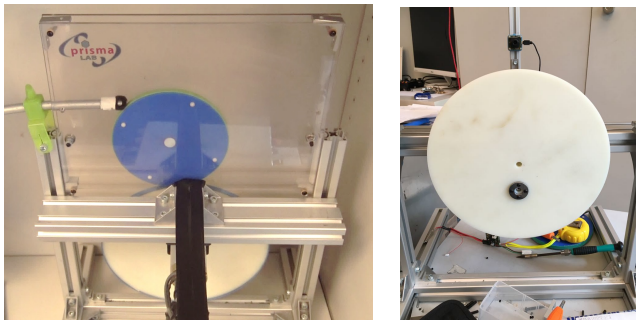

(a) The set-up is mounted in full-gravity between two plexiglass. Rubber bands of small thickness encircle both disks. On the left, a block allows the possibility to stop the upper disk to set the proper initial condition.

(b) A detail of the experimental set-up. It is possible to notice the displacement between the geometric center of the disk and its center of rotation attached to the motor shaft (black circle).

Fig. 8. Experimental prototype of the eccentric disk-on-disk system.

C. Experiments on the Eccentric Disk-on-Disk

The performance of the proposed IDA-PBC controller is evaluated on the experimental eccentric disk-on-disk set-up shown in Fig. 8(a). The lower disk (*i.e.*, the hand) is actuated by a DC Minertia R01SA motor, able to give a peak torque of 0.54 Nm and mounting an RSD-14B Harmonic Drive model whose gear-head ratio is $50:1$. With this configuration, it is possible to reach a continuous torque of 5.5 Nm with a maximum peak of 27 Nm, while the position accuracy is of about 13 arcsec. The rotation axis of the motor is placed at a distance $|\lambda|= 0.04$ m from the geometric center of the hand as shown in Fig. 8(b). The lower disk is homogeneous, and then the geometric center coincides with its CoM.

The control algorithm, coded in C++, runs on an external PC with a Linux-based operating system. A full-custom 120 W motor driver provides the motor commands. This device can give an accurate measure of the current as feedback thanks to an ad-hoc designed circuit, while the encoder signal is instead elaborated by a dedicated high-frequency device able to manage the considerable quantity of interrupts of the encoder. The feedback control signals are elaborated by an ARM CORTEX M3 microcontroller (32 bit, 75 MHz), on whose firmware the low-level inner control loop for the current runs at a frequency of 4 kHz. The microcontroller receives the inputs from the external PC through a universal serial bus. The low-level controller outputs the current reference for the motor servo, which provides the torque to the hand. Therefore, the torque u resulting from the IDA-PBC controller is transformed into a current reference, u_c, for the inner-control loop as

$$u_c = \frac{1}{k_m}(u+\mu_d\dot{\theta}_h+f_s\text{sign}(\dot{\theta}_h))+k_p(\hat{\theta}_h-\theta_h)+k_d(\dot{\hat{\theta}}_h-\dot{\theta}_h), \tag{44}$$

where $\hat{\theta}_h$ and $\dot{\hat{\theta}}_h$ are the desired hand position and velocity, respectively, obtained by integrating the following expression of the hand acceleration, resulting from the dynamics of the eccentric disk-on-disk derived in the subsection VIII-A,

$$\ddot{\hat{\theta}}_h = \left(\frac{b_{22}}{\Delta}\right)\left(u+\frac{b_{12}h_2}{b_{22}}-h_1\right), \tag{45}$$

where $h_1 = c_{11}\dot{\theta}_h + c_{12}\dot{s}_h + \nabla_{\theta_h}V$, $h_2 = c_{21}\dot{\theta}_h + c_{22}\dot{s}_h + \nabla_{s_h}V$, while the Coriolis terms are: $c_{11} = -\lambda m_o(\rho_h + \rho_o)\dot{s}_h \sin(s_h/\rho_h)/\rho_h$, $c_{12} = -\lambda m_o(\dot{s}_h + \dot{\theta}_h\rho_h)(\rho_h + \rho_o)\sin(s_h/\rho_h)/\rho_h^2$, $c_{21} = \lambda m_o(\rho_h+\rho_o)\dot{\theta}_h \sin(s_h/\rho_h)/\rho_h$, and $c_{22} = 0$. The gains and the parameters in (45) are experimentally tuned as $k_p = 3$, $k_d = 30$, the motor constant $k_m = 0.054$ Nm/A, the viscous friction coefficient $\mu_d = 0.13672$ Ns, and the torque required to overcome friction from rest $f_s = 0.2118$ Nm . The values of μ_d and f_s are found through some preliminary tests as in [11]. The microcontroller executes the computation of u_c at a frequency of 1 kHz.

A visual system provides the measurement of the angular position of the object, $\psi \in \mathbb{R}$, that is the angle that the center of the upper disk forms with respect to Σ_w, increasing counter-clockwise. This measure is elaborated from the geometry of the system to retrieve the current value of the arclength parameter of the hand: $s_h = \rho_h\left(\psi - \theta_h - \arcsin\left(\frac{\lambda}{\rho_o+\rho_h}\sin(\psi-\theta_h)\right)\right)$. The visual system consists of an uEye UI-122-xLE camera providing 360x340 pixel images to the PC at 75 Hz, which is also the high-level controller sample rate to compute u from the IDA-PBC controller. With the aim to increase the efficiency of the vision processing, the image elaboration algorithm focuses on an 80x80 pixel region of interest.

The values of the parameters of the eccentric disk-on-disk dynamic model are m_o = 0.224 Kg, m_h = 0.33 Kg, ρ_o = 0.075 m, ρ_h = 0.125 m, $I_o = m_o\rho_o^2$, $I_h = m_h\rho_h^2$, λ = -0.04 m, and g = 9.81 m/s^2.

In the following, two tests are carried out. The objective is to stabilize the equilibrium $\boldsymbol{q}^\star = (0,0)$. The controller gains are experimentally tuned as $k = -0.121$, $k_a = 2.05$, $k_v = 0.057$, and $k_f = 3550$. The video of the performed experiments is attached to the manuscript.

Notice that an open question is how generalizing the IDA-PBC approach to set constraints in the contact forces. For this reasons, the friction cones are not explicitly addressed in the formulation. This means that for particular choices of either control gains or initial condition of the system, the upper disk may slip or even loose contact with the lower disk. An analysis would be thus necessary to verify whether the continuous rolling assumption is satisfied during the entire experiments. Such analysis can be performed by empirically measuring the frictional coefficient between the two disks, and comparing it with the minimum frictional coefficient necessary to ensure rolling computed from the normal and frictional forces employing the measured experimental data. The procedure is detailed in [1] for the disk-on-disk set-up, and it is not reported here since it is out of the scope from the purposes of this paper.

1) Test 1: In this first test, the chosen initial conditions are $\theta_h(0) = 0$ rad, $\dot{\theta}_h(0) = 0$ rad/s, $s_h(0) = -0.01$ m, $\dot{s}_h(0) = 0$ m/s. Through these choices, the upper disk starts with an initial angle of about $\psi(0) \simeq -6$ deg with respect to the vertical axis of Σ_w.

Figure 9 shows the results obtained in this first experimental test. In particular, the figure depicts the time histories of $\theta_h(t)$, $\dot{\theta}_h(t)$, $s_h(t)$, $\dot{s}_h(t)$, $u(t)$, and $\psi(t)$. The plots show that the controller can balance the object at the upright unstable

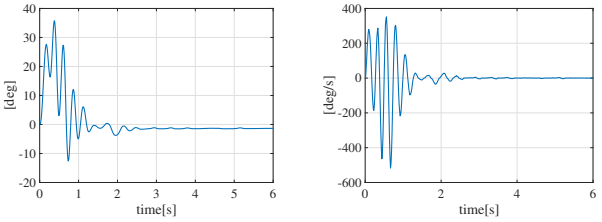

(a) Time history of $\theta_h(t)$.

(b) Time history of $\dot{\theta}_h(t)$.

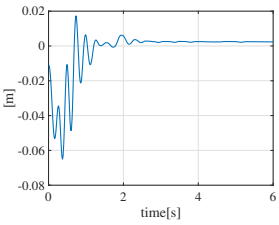

(c) Time history of $s_h(t)$.

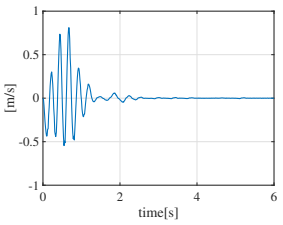

(d) Time history of $\dot{\theta}_h(t)$.

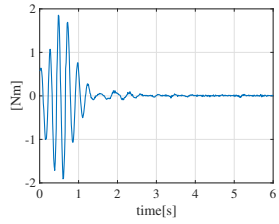

(e) Time history of $u(t)$.

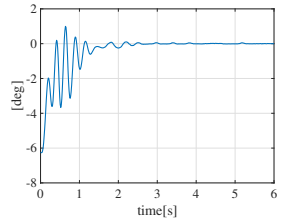

(f) Time history of $\psi(t)$.

Fig. 9. First experimental test for the eccentric disk-on-disk system controlled by the proposed IDA-PBC controller.

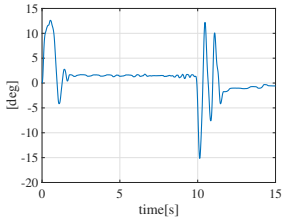

(a) Time history of $\theta_h(t)$.

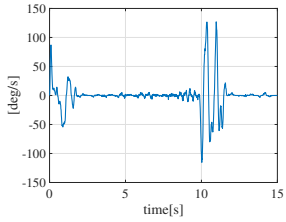

(b) Time history of $\dot{\theta}_h(t)$.

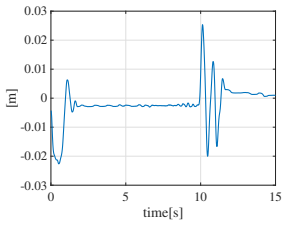

(c) Time history of $s_h(t)$.

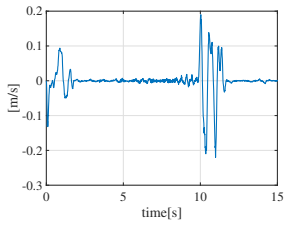

(d) Time history of $\dot{\theta}_h(t)$.

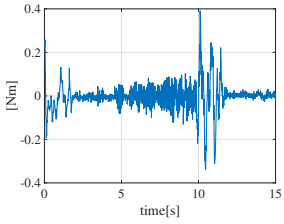

(e) Time history of $u(t)$.

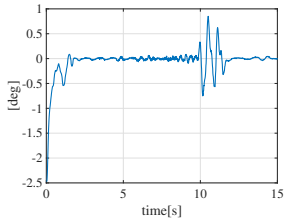

(f) Time history of $\psi(t)$.

Fig. 10. Second experimental test for the eccentric disk-on-disk system controlled by the proposed IDA-PBC controller.

position, see Fig. 9(f), while demanding a sufficiently smooth control torque, see Fig. 9(e). However, from Fig. 9(a) and Fig. 9(c), it is possible to notice that θ_h and s_h do not go exactly to zero, respectively, while instead, the angle ψ does. In particular, the steady-state value of θ_h is around 1.5 deg, while s_h is around 0.0024 m. These small errors are mainly due to calibration uncertainties of the vision system, plus some uncertainties on the model parameters. These last are rationally related to the experimental identification carried out to estimate the parameters of the motor.

2) Test 2: In this second test, the chosen initial conditions are $\theta_h(0) = 0$ rad, $\dot{\theta}_h(0) = 0$ rad/s, $s_h(0) = -0.0043$ m, $\dot{s}_h(0) = 0$ m/s. Through these choices, the upper disk starts with an initial angle of about $\psi(0) \simeq -2.5$ deg with respect to the vertical axis of Σ_w. The goal is the same as in the first test. Besides, the upper disk is voluntarily perturbed after around 10 s to test the robustness of the proposed control technique against external disturbances.

Figure 10 shows the results obtained in this second experimental test. As before, the figure depicts the time histories of $\theta_h(t)$, $\dot{\theta}_h(t)$, $s_h(t)$, $\dot{s}_h(t)$, $u(t)$, and $\psi(t)$. The plots show that the controller can balance the object at the upright unstable position, see Fig. 10(f), while demanding a sufficiently smooth control torque, see Fig. 10(e), and rejecting an external disturbance. The effects of the external perturbation are easily appreciable from all the plots. As for the first test, from Fig. 10(a) and Fig. 10(c), it is possible to notice that θ_h and s_h do not go exactly to zero, respectively, while instead, the angle ψ does. In particular, the steady-state value of θ_h is around -0.55 deg, while s_h is around 0.001 m. The same discussion regarding the source of the small steady-state error expressed in the *Test 1* applies also for the *Test 2*.

IX. Conclusion

A novel method to reduce the complexity of the IDA-PBC design is proposed in this paper. The achieved results can be applied to any underactuated mechanical systems expressed in the pH form, with both separable and non-separable Hamiltonians, whose dynamic model has dimension two. While the proposed approach aims at reducing the design complexity, it preserves the effectiveness of the IDA-PBC method. The proposed procedure employs a target potential energy matching equation, depending on a parametrization of the desired closed-loop mass matrix, to simultaneously simplify the identification of the desired mass matrix and select the desired energy function for the closed-loop system. The control methodology has been applied to the class of the nonprehensile planar rolling manipulation systems, overcoming some limitations appearing from a literature review. Two benchmark examples have been addressed: the ball-and-beam, and the eccentric disk-on-disk case studies. Simulations and experiments on the real physical set-up have been presented to evaluate the performance of the controllers.

Hence, the proposed methodology proposes a systematic procedure to design the control law for the broad class of underactuated mechanical planar system through the IDA-PBC framework, without explicitly solving the PDEs of the kinetic matching equation and providing a closed-form solution for the potential matching equation. The introduced design is also a generalization of [20] since it addresses non-separable Hamiltonian systems without the constraint that the hand must rotate around its center of mass: this means that is thus possible to solve a general nonprehensile planar rolling manipulation problem through the proposed IDA-PBC framework. The chosen benchmark examples highlight the benefit of employing the described methodology. In particular, it is possible to consider a more complicated, yet accurate, dynamic model for the ball-and-beam example rather than, for instance, in [3], [14]; while neither linearization nor simplification of the dynamic model is needed for the eccentric disk-on-disk example as in [24] and [25], respectively. Moreover, as remarked in Section V, the main result of the paper can be applied to any underactuated mechanical system with both separable and non-separable Hamiltonian. Academic examples that are not classifiable as nonprehensile manipulation case studies are the Acrobot and Pendubot system, the inertia-wheel pendulum, and the TORA system, with and without gravity.

Future extensions of this work aim at the development of analytical solutions to remove any potential singularity, which is inherited from the procedure proposed in [19]. Besides, the generalization to systems with higher dimensions than $n = 2$ and $m = 1$ (*i.e.*, 3D nonprehensile rolling manipulation systems exhibiting nonholonomic constraints [27], [28], [29], [30]) is indeed a current work.

APPENDIX I

In this appendix, given $V(q_1, q_2)$, $\alpha(q_1, q_2, \boldsymbol{c}_1)$, and $\boldsymbol{\beta}(q_1, q_2, \boldsymbol{c}_1)$, the explicit solution of (15) is provided for some particular cases. For the sake of clarity, given a generic function $f(a, b, c)$ of its arguments, the function $f(d, e, h)$ is computed by substituting $a = d$, $b = e$, and $c = h$. Some possible cases of interest are reported in the following, but the analysis can be extended.

Case 1. Consider $\alpha(q_1, q_2, \boldsymbol{c}_1) = k_1\gamma(q_1, q_2)$ and $\beta(q_1, q_2, \boldsymbol{c}_1) = k_2\gamma(q_1, q_2)$, with $k_1, k_2 \in \mathbb{R}$ and $\boldsymbol{\gamma}(q_1, q_2) \in \mathbb{R}$ a common function. This case is the one employed in Sections VII and VIII. The explicit solution is

$$V_d(\boldsymbol{q}, \boldsymbol{c}_2) = -\int_1^{q_1} \frac{\nabla_{q_2} V\left(\sigma, \frac{k_1 q_2 - k_2 q_1 + k_2 \sigma}{k_1}\right)}{k_1 \gamma\left(\sigma, \frac{k_1 q_2 - k_2 q_1 + k_2 \sigma}{k_1}\right)} \mathrm{d}\sigma + f\left(\frac{k_1 q_2 - k_2 q_1}{k1}, \boldsymbol{c}_2\right) \tag{46}$$

with $f(\cdot) \in \mathbb{R}$ any function of its arguments.

Case 2. Consider $\alpha(q_2, \boldsymbol{c}_1)$, $\beta(q_2, \boldsymbol{c}_1)$, and $V(q_2)$, that is they depend on the variable q_2 only. The explicit solution for this example is

$$V_d(\boldsymbol{q}, \boldsymbol{c}_2) = -\int_1^{q_2} \frac{1}{\beta(\sigma, \boldsymbol{c}_1)} \frac{\mathrm{d}V(\sigma)}{\mathrm{d}\sigma} \mathrm{d}\sigma + f\left(-q_1 + \int_1^{q_2} \frac{\alpha(\sigma, \boldsymbol{c}_1)}{\beta(\sigma, \boldsymbol{c}_1)} \mathrm{d}\sigma, \boldsymbol{c}_2\right). \tag{47}$$

Case 3. Consider $\alpha(q_1, q_2, \boldsymbol{c}_1) = 0$. The explicit solution for this example is

$$V_d(\boldsymbol{q}, \boldsymbol{c}_2) = -\int_1^{q_2} \frac{\nabla_{q_2} V(q_1, \sigma)}{\alpha(q_1, \sigma)} \mathrm{d}\sigma + f(q_1, \boldsymbol{c}_2). \tag{48}$$

Case 4. Consider $\beta(q_1, q_2, \boldsymbol{c}_1) = 0$. The explicit solution for this example is

$$V_d(\boldsymbol{q}, \boldsymbol{c}_2) = -\int_1^{q_1} \frac{\nabla_{q_2} V(\sigma, q_2)}{\alpha(\sigma, q_2)} \mathrm{d}\sigma + f(q_2, \boldsymbol{c}_2). \tag{49}$$

REFERENCES

[1] A. Donaire, F. Ruggiero, L. R. Buonocore, V. Lippiello, and B. Siciliano, "Passivity-based control for a rolling-balancing system: The nonprehensile disk-on-disk," *IEEE Transactions on Control System Technology*, vol. 25, no. 6, pp. 2135–2142, 2017.

[2] V. Duindam, A. Macchelli, S. Stramigioli, and H. Bruyninckx, *Modeling and control of complex physical systems: The port-Hamiltonian approach*. Springer Science & Business Media, 2009.

[3] F. Gómez-Estern, R. Ortega, F. Rubio, and J. Aracil, "Stabilization of a class of underactuated mechanical systems via total energy shaping," in *IEEE Conference on Decision and Control*, Orlando, FL, USA, 2001, pp. 1137–1143.

[4] R. Ortega, A. Donaire, and J. G. Romero, "Passivity-based control of mechanical systems," in *Feedback Stabilization of Controlled Dynamical Systems*, ser. Lecture Notes in Control and Information Sciences, N. Petit, Ed. Springer, 2017, vol. 473, ch. 7, pp. 167–199.

[5] R. Ortega, A. Van Der Schaft, B. Maschke, and G. Escobar, "Interconnection and damping assignment passivity-based control of port-controlled Hamiltonian systems," *Automatica*, vol. 38, no. 4, pp. 585–596, 2002.

[6] J. A. Acosta, R. Ortega, A. Astolfi, and A. M. Mahindrakar, "Interconnection and damping assignment passivity-based control of mechanical systems with underactuation degree one," *IEEE Transactions on Automatic Control*, vol. 50, no. 12, pp. 1936–1955, 2005.

[7] A. Donaire, R. Mehra, R. Ortega, S. Satpute, J. G. Romero, F. Kazi, and N. M. Singh, "Shaping the energy of mechanical systems without solving partial differential equations," *IEEE Transactions on Automatic Control*, vol. 61, no. 4, pp. 1051–1056, 2016.

[8] K. Nunna, M. Sassano, and A. Astolfi, "Constructive interconnection and damping assignment for port-controlled Hamiltonian systems," *IEEE Transactions on Automatic Control*, vol. 60, no. 9, pp. 2350–2361, 2015.

[9] D. Prattichizzo and J. Trinkle, "Grasping," in *Springer Handbook of Robotics*, B. Siciliano and O. Khatib, Eds. Springer International Publishing, 2016, pp. 955–988.

[10] J. Ryu, F. Ruggiero, and K. M. Lynch, "Control of nonprehensile rolling manipulation: Balancing a disk on a disk," in *IEEE International Conference on Robotics and Automation*, St. Paul, MN, USA, 2012, pp. 3232–3237.

[11] J. Ryu, F. Ruggiero, and K. M. Lynch, "Control of nonprehensile rolling manipulation: Balancing a disk on a disk," *IEEE Transactions on Robotics*, vol. 29, no. 5, pp. 1152–1161, 2013.

[12] F. Gordillo, J. Aracil, and F. Gómez-Estern, "Stabilization of autonomous oscillations and the hopf bifurcation in the ball and beam," in *IEEE Conference on Decision and Control*, Las Vegas, NV, USA, 2002, pp. 3924–3925.

[13] J. Hauser, S. Sastry, and P. Kokotovic, "Nonlinear control via approximate input-output linearization: The ball and beam example," *IEEE Transactions on Automatic Control*, vol. 37, no. 3, pp. 392–398, 1992.

[14] R. Ortega, M. Spong, F. Gómez-Estern, and G. Blankenstein, "Stabilization of a class of underactuated mechanical systems via interconnection and damping assignment," *IEEE Transactions on Automatic Control*, vol. 47, no. 8, pp. 1218–1233, 2002.

[15] K. Ryu and Y. Oh, "Balance control of ball-beam system using redundant manipulator," in *IEEE International Conference on Mechatronics*, Instanbul, TR, 2011, pp. 403–408.
[16] M. Cefalo, L. Lanari, and G. Oriolo, "Energy-based control of the butterfly robot," in *International IFAC Symposium on Robot Control*, Bologna, I, 2006, pp. 1–6.
[17] K. Lynch, N. Shiroma, H. Arai, and K. Tanie, "The roles of shape and motion in dynamic manipulation: The butterfly example," in *IEEE International Conference on Robotics and Automation*, Lueven, BE, 1998, pp. 1958–1963.
[18] M. Surov, A. Shiriaev, L. Freidovich, S. Gusev, and L. Paramonov, "Case study in non-prehensile manipulation: Planning perpetual rotations for "Butterfly" robot," in *IEEE International Conference on Robotics and Automation*, Seattle, WA, USA, 2015, pp. 1484–1489.
[19] M. Ryalat and D. Laila, "A simplified IDA–PBC design for underactuated mechanical systems with applications," *European Journal of Control*, vol. 27, pp. 1–16, 2016.
[20] V. Lippiello, F. Ruggiero, and B. Siciliano, "The effects of shapes in input-state linearization for stabilization of nonprehensile planar rolling dynamic manipulation," *IEEE Robotics and Automation Letters*, vol. 1, no. 1, pp. 492–499, 2016.
[21] F. Ruggiero, V. Lippiello, and B. Siciliano, "Nonprehensile dynamic manipulation: A survey," *IEEE Robotics and Automation Letters*, vol. 3, no. 3, pp. 1711–1718, 2018.
[22] A. Teel and L. Praly, "Tools for semiglobal stabilization by partial state and output feedback," *SIAM Journal on Control and Optimization*, vol. 33, no. 5, pp. 1443–1488, 1995.
[23] Y. Aoustin and A. Formal'sky, "Beam-and-ball system under limited control: Stabilization with large basin of attraction," in *IEEE American Control Conference*, St Louis, MO, USA, 2009, pp. 555–560.
[24] Y. Aoustin and A. Formal'sky, "An original circular ball-and-beam system: stabilization strategy under saturating control with large basin of attraction," in *European Control Conference*, Kos, GR, 2007, pp. 4833–4838.
[25] S. Satpute, R. Mehra, F. Kazi, and N. Singh, "Geometric–PBC approach for control of circular ball and beam system," in *International Symposium on Mathematical Theory of Networks and Systems*, Groningen, NL, 2014, pp. 1238–1243.
[26] J. Hauser, S. Sastry, and P. Kokotovic, "Nonlinear control via approximate input-output linearization: The ball and beam example," *IEEE Transactions on Automatic Control*, vol. 37, no. 3, pp. 392–398, 1992.
[27] A. Bicchi and A. Marigo, "Dexterous grippers: Putting nonholonomy to work for fine manipulation," *The International Journal of Robotics Research*, vol. 21, no. 5-6, pp. 427–442, 2002.
[28] V. Duindam and S. Stramigioli, "Modeling the kinematics and dynamics of compliant contact," in *IEEE International Conference on Robotics and Automation*, Taipei, TW, 2003, pp. 4029–4034.
[29] A. Gutiérrez-Giles, F. Ruggiero, V. Lippiello, and B. Siciliano, "Nonprehensile manipulation of an underactuated mechanical system with second-order nonholonomic constraints: The robotic hula-hoop," *IEEE Robotics and Automation Letters*, vol. 3, no. 2, pp. 1136–1143, 2018.
[30] K. Lee, G. Batz, and D. Wollherr, "Basketball robot: Ball-on-plate with pure haptic information," in *IEEE International Conference on Robotics and Automation*, Pasadena, CA, USA, 2008, pp. 2410–2415.

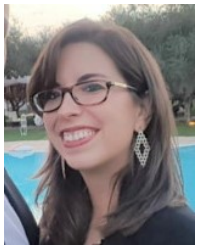

Diana Serra received the Ph.D. degree in Information Technology and Electrical Engineering at the University of Naples Federico II in 2017. Her main research interests are: passivity-based and optimal control theory applied to mobile and service robotics. Currently, she is a technology innovation specialist in the Research and Development division of Rete Ferroviaria Italiana s.p.a.

Fabio Ruggiero received the M.Sc. degree in Automation Engineering from the University of Naples Federico II in 2007. He got the Ph.D. degree from the same institution in 2010. He spent seven months at Northwestern University as a visiting Ph.D. student from September 2009 to March 2010. After several PostDoctoral positions from 2011 to 2016, he has been holding an Assistant Professor position at the University of Naples Federico II. His research interests are focused on dexterous and dual-hand robotic manipulation, even by using UAVs with small robotic arms, dynamic nonprehensile manipulation, 3D object preshaping and reconstruction. He has co-authored about 50 among journal papers, book chapters, and conference papers.

Alejandro Donaire received his degree in Electronic Engineering in 2003 and his Ph.D. in 2009, both from the National University of Rosario. In 2009, he took a research position at the Centre for Complex Dynamic Systems and Control at The University of Newcastle, and in 2011 he was awarded the UON Postdoctoral Research Fellowship. In March 2015, he joined the PRISMA Lab at University of Naples Federico II where he worked for two years. In 2017, he joint the Institute for Future Environments at the Queensland University of Technology (QUT), where he worked as Senior Research Fellow. Since 2019, he is with the School of Engineering at the University of Newcastle and conducts his academic activities within the Mechatronic Discipline. His research interests include nonlinear dynamics, control theory and system design for robotics, mechatronics, marine and aerospace applications.

Luca Rosario Buonocore received the Ph.D. degree in Computer and Automation Engineering at the University of Naples Federico II in 2015. His main research interests are: mechatronic design of novel robotic solutions, like mobile robotic platforms and ultralight robotic arms for areal manipulation. Currently, he is a research fellow at CERN in R&D robotic division of engineering group.

Vincenzo Lippiello was born in Naples, Italy, on June 19, 1975. He received his Laurea degree in electronic engineering and the Research Doctorate degree in information engineering from the University of Naples Federico II, in 2000 and 2004, respectively. He is an Associate Professor of Automatic Control in the Department of Electrical Engineering and Information Technology, University of Naples Federico II. His research interests include visual servoing of robot manipulators, hybrid visual/force control, adaptive control, grasping and manipulation, aerial robotics, and visual object tracking and reconstruction. He has published more than 120 journal and conference papers and book chapters.

Bruno Siciliano is Director of the Interdepartmental Center for Advances in RObotic Surgery (ICAROS), as well as Coordinator of the Laboratory of Robotics Projects for Industry, Services and Mechatronics (PRISMA Lab), at University of Naples Federico II. Fellow of the scientific societies IEEE, ASME, IFAC, he received numerous international prizes and awards, and he was President of the IEEE Robotics and Automation Society from 2008 to 2009. Since 2012 he is on the Board of Directors of the European Robotics Association. He has delivered more than 150 keynotes and has published more than 300 papers and 7 books. His book "Robotics" is among the most adopted academic texts worldwide, while his edited volume "Springer Handbook of Robotics" received the highest recognition for scientific publishing: 2008 PROSE Award for Excellence in Physical Sciences & Mathematics. His research team got 16 projects funded by the European Union for a total grant of 10 M in the last ten years, including an Advanced Grant from the European Research Council.